ISSN Online: 2349-7777

Development of Structure Activity Correlation Model on 4-Quinolones Derivatives as Tubulin Polymerization Inhibitors: Rationale to Advance the Understanding of Structure Activity Profile

Vijay K. Patel [1], Avineesh Singh [1], Deepak K. Jain [1], Ajay K. Sharma [2], Arun K Gupta [3], Prabodh C Sharma [4], Harish Rajak [1]*

[1] Medicinal Chemistry Research Laboratory, SLT Institute of Pharmaceutical Sciences, Guru Ghasidas University, Bilaspur-495 009, (CG) India
[2] Department of Pharmacy, G.S.V.M., Medical College, Kanpur-208002, (UP) India
[3] B.P.S. Mahila Vishwavidyalaya, Khapur-Kalan, Sonepat-131 001, (Haryana) India
[4] Institute of Pharmaceutical Sciences, Kurukshetra University, Kurukshetra-136 119, (Haryana) India

Received 28 October 2013; accepted in revised form 19 December 2013

Abstract: Three-dimensional quantitative structure-activity relationship (3D-QSAR), pharmacophore studies and docking studies was performed on a series of 4-Quinolones derivatives as antitumor agent and structure activity correlation was established. Subsequent ADME studies disclosed the pharmacokinetic efficiency of these compounds. 3D-QSAR models were generated using a set of 43 compounds of 4-Quinolones derivatives as inhibitor of tubulin polymerization for antitumor activity. Five-point common pharmacophore hypotheses were chosen for alignment of all compounds. The 3D-QSAR models generated using training set (31 compounds) and test set (12 compounds) exhibited good partial least squares statistical results. The developed common pharmacophore hypothesis (CPHs) and 3D-QSAR models were validated further externally by predicting the activity of database of compounds and comparing it with actual activity. We have selected the 3D-QSAR models generated by CPHs AADRR.11 for correlating the structure with activity. Docking studies were also performed for all compounds on colchicine binding site of β tubulin for examine the binding affinity of compounds for antitumor activity. ADME properties studies predict both physiochemically noteworthy descriptors and pharmacokinetically relevant properties extremely useful in the context of both high-throughput library screening and lead optimization. The results of these molecular modeling studies are helpful to improve the pharmacophore for design of novel potential compounds for antitumor activity.

Key words: 3D-QSAR, Pharmacophore, Combretastatin A-4, 4-Quinolones, Common Pharmacophore Hypothesis.

Introduction

Microtubules are involved in a wide number of cellular functions, such as division, motility, intracellular transport and shape maintenance. The major protein component found in microtubules is tubulin. Interference with microtubule assembly, either by inhibition of tubulin polymerization or by blocking microtubule disassembly, leads to an increase in the number of cells in Metaphase arrest. Inhibition of microtubule function using tubulin targeting agents is a validated approach to anticancer

*Corresponding author (Harish Rajak)
E-mail: < harishdops@yahoo.co.in >

therapy [1-5]. A series of 4-Quinolones as a new class of antimitotic antitumor agents are potent tubulin assembly inhibitors that bind to the colchicine site on β tubulin close to its interface with α tubulin within the α,β dimer. 4-Quinolones efficiently inhibit tubulin polymerization and cancer cell growth, with activities comparable with those of colchicine and Combretastatin A-4 (CA-4) [6].

CA-4 (Fig. 1) is a low molecular weight natural product that binds to the colchicine site of tubulin. Combretastatins are mitotic agents isolated from the bark of the South African tree *Combretum caffrum* [7-9]. The most potent combretastatin A-4 (CA-4) [20, *cis*-1-(3,4,5-trimethoxyphenyl)-2-(3'-hydroxyl-4'-methoxyphenyl)ethane] is a simple stilbene that has been shown to compete with colchicines for binding sites on tubulin. It has been found to be a potent cytotoxic agent, which strongly inhibits the polymerization of tubulin by binding to the colchicine site. CA-4 was described as a strong cell growth and tubulin inhibitor [10]. CA-4 is thus an attractive lead molecule for the development of anticancer drugs [11-13]. CA-4 Phosphate (CA-4-P) and ombrabulin (Fig. 1) are currently being investigated in a number of clinical trials. Ombrabulin was granted orphan drug status by the European Medicines Agency in April 2011.

In search of novel targets using computational studies, we present here the correlation of structures of 4-Quinolones (Fig. 1) derivatives with inhibition of tubulin polymerization (ITP). In order to optimize this pharmacophore and for further improving the activity, we developed atom based 3D-QSAR models using pharmacophore align-ment and scoring engine (PHASE), performed docking study on colchicines binding site of β tubulin using grid based ligand docking with energetics (GLIDE) and predict ADME characteristics by using Qikprop. PHASE is a comprehensive, self contained system for pharmacophore perception, QSAR model development, and 3D database screening [14]. The GLIDE docking module approximated a complete systematic search of the conformational, orientation and positional space of the docked ligand molecules into the receptor-binding pocket [15]. Qikprop is a tool to predict ADME properties. It predicts both physiochemically important descriptors and pharmacokinetically applicable properties tremendously useful in the perspective of high-throughput library screening and lead optimization.

The developed atom based 3D-QSAR model, docking studies emphasizes the structural features of 4-Quinolones analogous of CA-4 for binding to colchicines binding site of β tubulin and ADME studies indicated the pharmacokinetic efficiency of these compounds which might be beneficial for further design of more potent tubulin binding agent with pharmacokinetic competence.

Materials and methods

Biological data

A set of 43 dataset of 4-Quinolones derivative (Table 1a, 1b, 1c) with available IC_{50} (μM) data for cytotoxic activity against ITP were taken from literature [6] for the development of ligand based CPHs. The IC_{50} values (in moles/liter) was converted into negative logarithm of IC_{50} (pIC_{50}) was used in this study. For 3D-QSAR studies, these 43 com-pounds were divided into a training set (31 compounds) and a test set (12 compounds). The training set molecules were selected randomly in such a way that they contained information in redundant

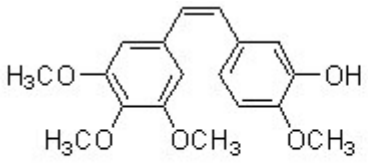

Combretastatin A-4 (CA-4)

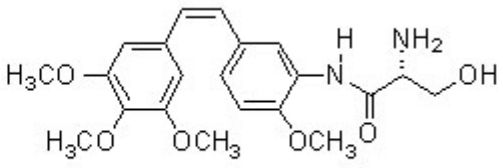

Ombrabulin (Clinical Trail)

Fig.1 Chemical Structure of CA-4 and Ombrabulin

Table 1a. Structure of 2',3',4',5',6,7-Substituted 2-Phenyl-4-quinolones used for development of common pharmacophore hypothesis and 3D-QSAR studies along with biological activity

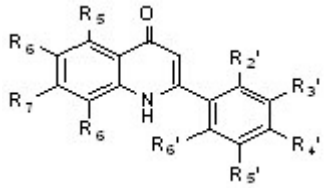

Comp.	$R_{2'}$	$R_{3'}$	$R_{4'}$	$R_{5'}$	R_6	R_7	ITP IC_{50} (μM)
1	H	H	H	H	OCH_2O		0.63
2	H	H	OCH_3	H	OCH_2O		40
3	H	OCH_3	H	H	OCH_2O		0.57
4	OCH_3	H	H	H	OCH_2O		14
5	H	OPh	H	H	OCH_2O		40
6	H	H	N(CH3)2	H	OCH_2O		40
7	H	N(CH3)2	H	H	OCH_2O		0.7
8	H	H	CH_3	H	OCH_2O		1.0
9	H	OCH_3	OCH_3	H	OCH_2O		40
10	H	OCH_3	H	OCH_3	OCH_2O		0.62
11	OCH_3	H	OCH_3	H	OCH_2O		40
12	OCH_3	H	H	OCH_3	OCH_2O		5.5
13	H		OCH_2O	H	OCH_2O		1.1
14	H	OCH_3	OCH_3	OCH_3	OCH_2O		40
15	OCH_3	OCH_3	OCH_3	H	OCH_2O		40
16	F	H	H	H	OCH_2O		0.85
17	Cl	H	H	H	OCH_2O		0.89
18	H	$N(CH_3)_2$	H	H	H	H	1.5
19	H	H	$N(CH_3)_2$	H	H	H	40
20	H	OCH_3	H	H	H	H	1.4
21	H	OCH_3	OCH_3	OCH_3	H	H	40
22	H	H	H	H	OCH_3	OCH_3	18
23	H	$N(CH_3)_2$	H	H	OCH_3	OCH_3	15
24	H	OCH_3	H	H	OCH_3	OCH_3	4.3
25	H	OCH_3	OCH_3	H	OCH_3	OCH_3	40
26	H	H	OCH_3	H	OCH_3	H	40
27	H	H	OH	H	OCH_3	H	5.6
28	H	H	OCH_3	H	H	H	40
29	H	H	OCH_3	H	H	F	40
30	H	$N(CH_3)_2$	H	H	OCH_3	H	0.84
31	H	OCH_3	H	H	OCH_3	H	0.74

terms of both their structural features and biological activity ranges.

The most active molecules, moderately active, and less active molecules were included in training set to spread out the range of activities. In order to assess the predictive power of the model, a set of 12 compounds was arbitrarily set aside as the test set. The test compounds were selected in such a way that they truly represent the training set.

Table 1b. Structure of 5,6,7-Substituted 2-Heterocyclic 4-Quinolones and a Related Styryl Derivative used for development of common pharmacophore hypothesis and 3D-QSAR studies along with biological activity

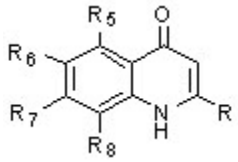

Comp.	R'	R5	R6	R7	ITP IC_{50} (μM)
32	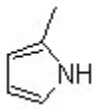	H	OCH_2O		18
33	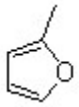	H	OCH_2O		23
34		H	OCH_2O		2.2
35	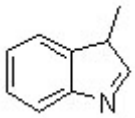	H	OCH_2O		1.3
36	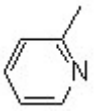	H	H	F	40
37	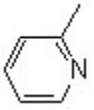	F	H	H	40
38	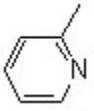	H	OCH_3	H	40
39	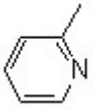	H	Cl	H	40
40	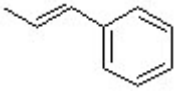	H	OCH_2O		2.3

Ligand preparation

The structure of each compounds were cleaned and optimized using Ligprep v2.6 (Schrodinger, LLC, New York, NY, 2012). The cleanup and optimization process include conversion of structures from 2D to 3D, addition of hydrogen atoms, removal of counter ions, ionization state at the pH 7.0, generation of stereoisomer's, removal of noncompliant structures, and energy minimization. Conforms of all ligands were generated using conformer generation macromodel search method [16] with maximum number of conformers 1,000 per structure and minimization steps 100 and minimized using OPLS_2005 force field [17] each minimized conformer was further filtered to eliminate

Table 1c. Structure of 2',3'-Fueed 6,7-(Methylenedioxy)-2-phenyl-4-quinolones used for development of common pharmacophore hypothesis and 3D-QSAR studies along with biological activity

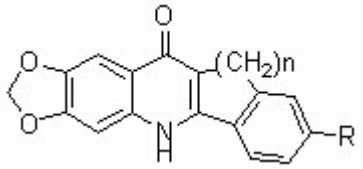

Compound	n	R	ITP IC_{50} (μM)
41	2	H	40
42	2	OCH_3	400
43	3	H	40

conformations. For each molecule, a set of conformers with maximum energy difference of 10 kcal/mol relative to global energy minimum conformers were retained. The conformer generation studies are based on methods i.e., torsion sampling or mixed Monte-Carlo Multiple Minimum (MCMM)/Low Mode (LMOD), where the minimized structures are finally obtained through a filter using defined relative energy window, typically of 10 kcal/mol. Also, conformers with the RMSD of lower than 1.0 A° between all pairs of corresponding heavy atoms were considered identical and rejected.

Pharmacophore modeling

Pharmacophore modeling and 3-D database searching are now recognized as integral components of lead discovery and lead optimization. The continuing need for improved pharmacophore based tools has driven the development of 'PHASE'v3.4 (Schrodinger, LLC, New York, NY, 2012). To reach our research objectives we have used 'PHASE': a module of Schrodinger's drug design software.

Generation of the common pharmacophore hypotheses (CPHs)

The CPHs was carried out by PHASE [14]. Pharmacophore features; hydrogen bond acceptor (A), hydrogen bond donor (D), hydrophobic group (H), negatively charged group (N), positively charged group (P) and aromatic ring (R) were defined by a set of chemical structure patterns as SMARTS queries. Common pharmacophoric features were then identified from a set of variants (set of feature types) that define a possible pharmacophore using a tree-based partitioning algorithm with maximum tree depth of four with the requirement that all actives must match. After applying default feature definitions to each ligand, CPHs were generated using a final box of 1 A°. All generated CPHs were examined and selected based on a scoring function to yield the best alignment of the active ligands using an overall maximum root mean square deviation (RMSD) value of 1.2 A° with default options for distance tolerance. The quality of alignment was measured by a survival score. Defined as:

$$S = W_{site}S_{site} + W_{vec}S_{vec} + W_{vol}S_{vol} + W_{sel}S_{sel} + W^{m}_{rew} - W_{E}\Delta E + W_{act}A$$

where, W's are weights and S's are scores; S_{site} represents alignment score, the RMSD in the site point position; S_{vec} represents vector score, and averages the cosine of the angles formed by corresponding pairs of vector features in aligned structures; S_{vol} represents volume score based on overlap of vanderwaals models of non hydrogen atoms in each pair of structures; and S_{sel} represents selectivity score and accounts for what fraction of molecules are likely to match the hypothesis regardless of their activity towards the receptor. W_{site}, W_{vec}, W_{vol} have default values of 1.0, while W_{sel} has a default value of 0.0. In hypothesis generation, default values have been used. The

reward comes in the form of W^m_{rew} where W_{rew} is user-adjustable (1.0 by default) and m is the number of actives that match the hypothesis minus one. $W_E\Delta E$ represents penalty included for high energy structures by subtracting a multiple of the relative energy from the final score and penalize hypothesis for which the reference ligand activity is lower than the highest activity, by adding a multiple of the reference ligand activity to the score represented by $W_{act}A$, where A is the activity. The CPHs with high survival score were chosen for alignment of molecules and used for further 3D-QSAR studies.

Building of 3D-QSAR models

An atom based 3D-QSAR model is more useful in explaining the structure activity relationship than pharmacophore based 3D-QSAR as latter do not consider ligand features beyond the pharmacophore model. In atom-based 3D-QSAR, a molecule is treated as a set of overlapping vanderwaals spheres. Each categories according to a simple set of rules: hydrogens attached to polar atoms are classified as hydrogen bond donors (D); carbons, halogens, and C–H hydrogens are classified as hydrophobic/non-polar (H); atoms with an explicit negative ionic charge are classified as negative ionic (N); atoms with an explicit positive ionic charge are classified as positive ionic (P); non ionic atoms are classified as electron withdrawing (W); and all other types of atoms are classified as miscellaneous (X). For construction of atom based 3D-QSAR model, a rectangular grid of cubes (1 A° on each side) were defined for aligned training set for occupation of all atoms. Each occupied cubes were allotted one or more volume bits to represent the molecules by string of zero and ones. This representation gives rise to binary valued occupation patterns that was used as independent variables to create PLS QSAR models [14]. The PLS regression was carried out with maximum of N/5 PLS factors, where N is the number of ligands in training set.

Validation of pharmacophore model

Validation is a crucial aspect of pharmacophore design, particularly when the model is built for the purpose of predicting activities of molecules in test series. In the present case, the developed pharmacophore model was validated by predicting the activity of test set molecules. The correlation between the experimental and predicted activities of the test set molecules was determined. We accept models with Q^2 values for the training set greater than 0.5 and R^2 values for predicted versus actual activities of the test set compounds greater than 0.6 [18, 19].

Docking method

The molecular docking tool, Glide v5.8 (Schrodinger, LLC, New York, NY, 2012) was used for docking studies of all compounds on colchicines binding site of β tubulin. The crystal structure of β tubulin was acquired from protein data bank (PDB code: 1SA0) and was made ready for docking using ‘‘protein preparation wizard’’ in Maestro wizard v9.3 (Schrodinger, LLC, New York, NY, 2012). Water molecules in the crystal structures were removed. The protein preparation was performed in two steps, preparation and refinement. In preparation phase, after confirming chemical correctness, the hydrogen atoms were added where hydrogen atoms were missing. Side chains that are not close to the binding cavity and do not contribute in salt bridges were neutralized. In the refinement phase, a restrained impact minimization of the co-crystallized complex was carried out. This helps in reorientation of side chain hydroxyl group. It utilizes the OPLS_2005 force field for this purpose. Grids were defined by centering them on the ligand in the crystal structure using the default box size.

The ligands were built using maestro build panel and prepared by Ligprep which produces the low energy conformer of ligands using OPLS_2005 force field [16-17]. The lower energy conformations of the ligands were selected and docked into the grid generated from protein structures using Extra Precision (XP) docking mode. Compounds were sorted on the basis of docking score to furnish only those hits which significantly interacted with the colchicine site on β tubulin. Evaluation was done with glide score (docking score) and the single best pose is generated as the output for particular ligand.

GScore is expressed as

Gscore = a x vdw + b x coul + Lipo + H – bond + Metal + BuryP + RotB + Site

where, vdW is Vander Waal energy, Coul is Coulomb energy, Lipo is lipophilic contact term, H-bond is hydrogen bonding term, Metal is metal binding term, BuryP is the penalty for buried polar groups, RotB is the penalty for freezing rotatable bonds, Site is polar interactions at the active site, and the Coefficients of vdW and Coul are a = 0.065, b = 0.130. Chem score and atom-atom pair function assigns scores to lipophilic ligand atoms based on summation over a pair function each term of which depends on the interatomic distance between a ligand atom and a neighboring lipophilic protein atom [20-23].

ADME studies

ADME properties were calculated using Qikprop v3.5 (Schrodinger, LLC, New York, USA). It aid in calculating important physiochemical descriptors and appropriate pharmacokinetic properties useful in lead optimization and high-throughput library screening. It also evaluates the acceptability of analogs based on the Lipinski rule of five, which is essential to ensure drug-like pharmacokinetic profile while using rational drug design [24, 25]. All the analogs were neutralized before being used by Qikprop.

Results and discussion

Generation of 3D-QSAR models

The active and inactive thresholds were set as 6.00 and 4.5 respectively. The pharmacophoric features present for creating sites were hydrogen bond acceptor (A), hydrogen bond donor (D) and aromatic ring (R) hydrophobic group (H). Different variant CPHs were generated by common pharmacophore identification process. The five featured pharmacophore hypotheses were high value of survival score, able to define the complete binding space of the selected molecules. Five featured pharmacophore hypotheses were selected and subjected to rigorous scoring function. The two hypothesis (AADRR.11 and AADRR.12) were employed for the 3D-QSAR study and characterized by survival score (Table 2).

All top CPHs (AADRR.11 and AADRR.12) were used for atom-based 3D-QSAR model generation. The good CPHs yielded a 3D-QSAR model with good value of regression coefficient, low standard deviation and high variance ratio with good stability, good predictive power, low RMSE value and high Pearson R value which stands for correlation between predicted and observed activity for test set. We selected two dissimilar 3D-QSAR models generated by CPHs, AADRR.11 and AADRR.12 for correlating the structure with activity.

The CPHs AADRR.11 and AADRR.12 produced 3D-QSAR models with good PLS statistical values **(**Table 3). These hypotheses exhibited good internal as well as external predictive power. The training set correlation in both CPHs is characterized by PLS factors R^2 = 0.9341, SD = 0.1995, F = 92.1, P = 5.806e-015, Q^2 = 0.8687 for CPH AADRR.11, and R^2 = 0.9366, SD = 0.1958, F = 95.9, P = 3.558e-015, Q^2 = 0.7595 for CPH AADRR.12. The test set correlation is characterized by PLS factors R^2 =0.64 (Fig. 2b), RMSE =0.3209, Pearson R = 0.9647 for CPH AADRR.11 and R^2 =0.50, RMSE =0.4343, Pearson R = 0.9502 for CPH AADRR.12. We accept models with Q^2 values for the training set greater than 0.5 and R^2 values for predicted versus actual activities of the test set compounds greater than 0.6 thus model AADRR.11 was accepted and AADRR.12 was rejected.

Table 2. Survival score of top five CPHs

S. No.	CPHs	Survival	Site	Vector	Volume	Inactive	Survival-Inactive
1	AADRR.11	3.779	0.98	0.932	0.871	2.541	1.238
2	AADRR.12	3.636	0.83	0.948	1.489	2.441	1.177

Table 3. Statistical results of 3D-QSAR model developed using different CPHs

S. No.	Statistic parameters	3D- QSAR models	
		AADRR.11	AADRR.12
1	SD	0.1995	0.1958
2	R^2	0.9341	0.9366
3	F	92.1	95.9
4	P	5.806e-015	3.558e-015
5	Stability	0.625	0.459
6	RMSE	0.3209	0.4343
7	Q^2	0.8687	0.7595
8	Pearson	0.9647	0.9502

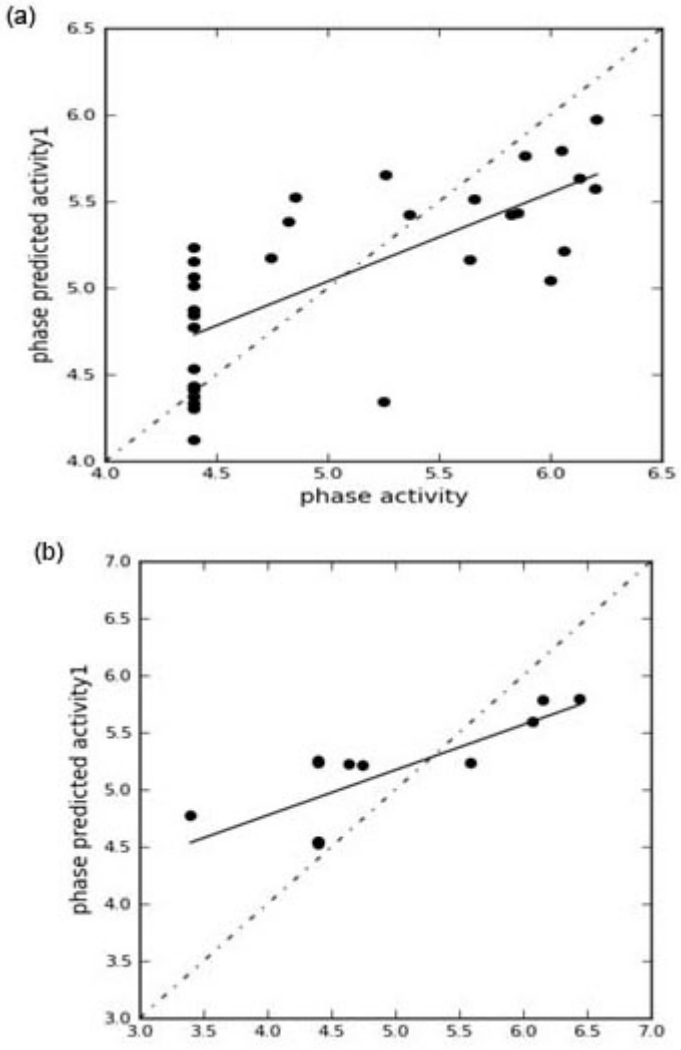

Fig. 2 Plot of phase activity versus predicted activity for 3 D-QSAR model generated using CPHs: CPHs: AADRR.11 (a) training set R^2 =0.56 (b) test R^2 =0.64

The fitness scores for all ligands were examined on the best scored pharmacophore model. The greater the fitness score, the greater the activity prediction of the compound. The fit function does not only check if the feature is mapped or not, it also contains a distance term, which determines the distance that separates the feature on the molecule from the centroid of the hypothesis feature. Table 4 indicates the fitness score for all the molecules of training set.

3-D QSAR analysis

The 3D-QSAR models developed using CPHs AADRR.11 were applied to database of compounds considered from literature (Li et al., 1994**)** for validation purpose. The activity of these reported compounds having 4-Quinolones or similar pharmacophoric group were predicted and compared with its actual activity (Table 4). The residual values obtained by subtraction of predicted activity from reported activity was found to be near zero for number of compounds. The mean of residual was also calculated and found as -1.538 for 3D-QSAR models associated with CPHs AADRR.11. 3D-QSAR models based on the molecules of training and test set using various features, i.e., hydrogen bond donor, hydrogen bond acceptors and hydrophobic group has been studied. A pictorial representation of the cubes generated in the present 3D-QSAR is shown in Figs. 3, 4 and 5. In these generated cubes, the blue cubes indicate favorable features, while red cubes indicate unfavorable features for biological activity. The antitumor activity can be achieved by visualizing the 3D-QSAR model in the context of one or more ligands in the series with changing activity. This information can be employed to design novel or more active analogues.

Table 4 Comparison of observed biological activity and predicted activity along with fitness of compounds on CPHs

Comp.	Actual pIC_{50}	3D QSAR model AADRR.11		
		Predicated pIC_{50}	Residue	Fitness
1	6.201	5.71	0.491	3
2	4.398	4.67	-0.272	2.942566
3*	6.244	6.18	0.064	2.941994
4	4.854	4.99	-0.136	2.898265
5	4.398	4.58	-0.182	2.549533
6	4.398	4.72	-0.322	2.67143
7*	6.155	5.97	0.185	2.905997
8	6	5.9	0.1	2.730525
9*	4.398	5.11	-0.712	2.890907
10	6.208	6.22	-0.012	2.892853
11	4.398	4.38	0.018	2.853996
12	5.26	5.04	0.22	2.847262
13*	5.959	5.33	0.629	2.904051
14	4.398	4.54	-0.142	2.843708
15*	4.398	4.73	-0.332	2.813044
16	6.071	5.8	0.271	2.682186
17	6.051	6.14	-0.089	2.904037
18	5.824	5.72	0.104	2.360332
19*	4.398	4.63	-0.232	2.361123
20	5.854	5.95	-0.096	2.393619
21	4.398	4.38	0.018	0.900304
22*	4.745	4.83	-0.085	2.779701
23	4.824	4.98	-0.156	2.702959
24	5.367	5.24	0.127	2.730894

table 4. (continued).

Comp.	Actual pIC_{50}	3D QSAR model AADRR.11		
		Predicated pIC_{50}	Residue	Fitness
25	4.398	4.18	0.218	2.687596
26*	4.398	4.5	-0.102	2.725919
27	5.252	4.89	0.362	2.53596
28	4.398	4.25	0.148	2.420715
29	4.398	4.32	0.078	2.426789
30*	6.076	6.17	-0.094	2.572362
31	6.131	6.37	-0.239	2.601817
32	4.746	4.69	0.056	2.797742
33*	4.638	4.89	-0.252	2.775523
34	5.658	5.69	-0.032	2.872337
35	5.886	5.96	-0.074	2.427506
36	4.398	4.46	-0.062	2.267867
37*	4.398	4.48	-0.082	2.223549
38	4.398	4.48	-0.082	2.65038
39	4.398	4.3	0.098	2.263354
40	5.638	5.81	-0.172	2.349458
41	4.398	4.46	-0.062	2.884166
42*	3.398	3.94	-0.542	2.838445
43	4.398	4.56	-0.162	2.598389

* Compounds in test set

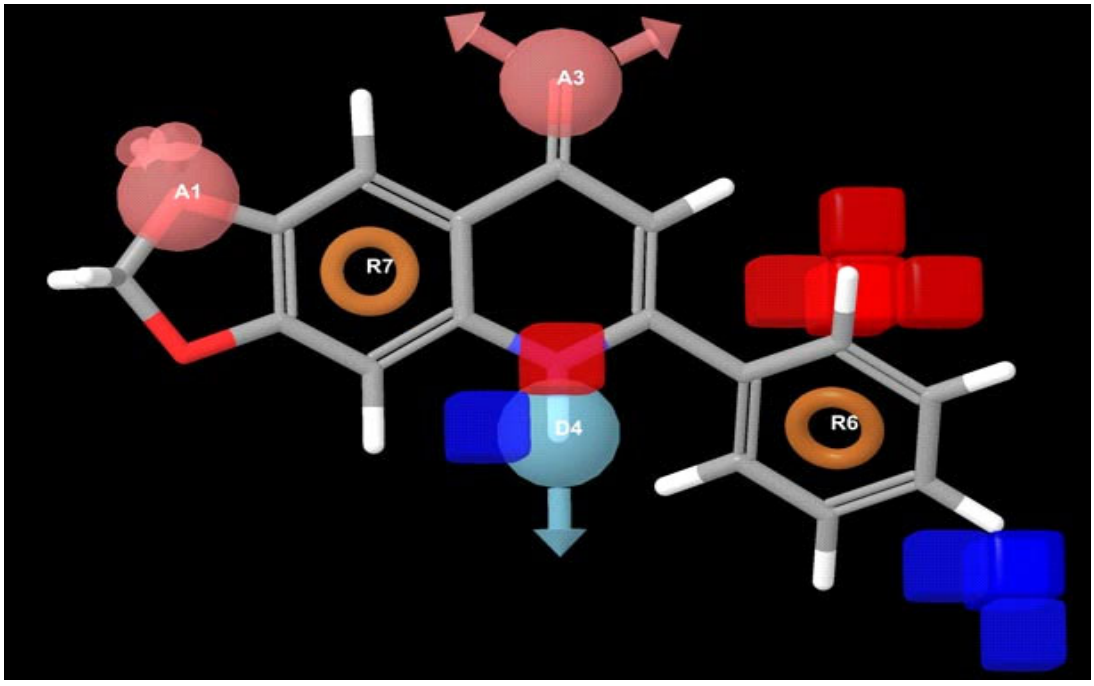

Fig. 3. Pictorial representation of the cubes generated using the 3-D QSAR model based on Comp. no. 1 of training set illustrating hydrogen bond donor feature CPHs: AAHRR.11. Blue cubes indicate favorable regions, while red cubes indicate unfavorable region for the activity

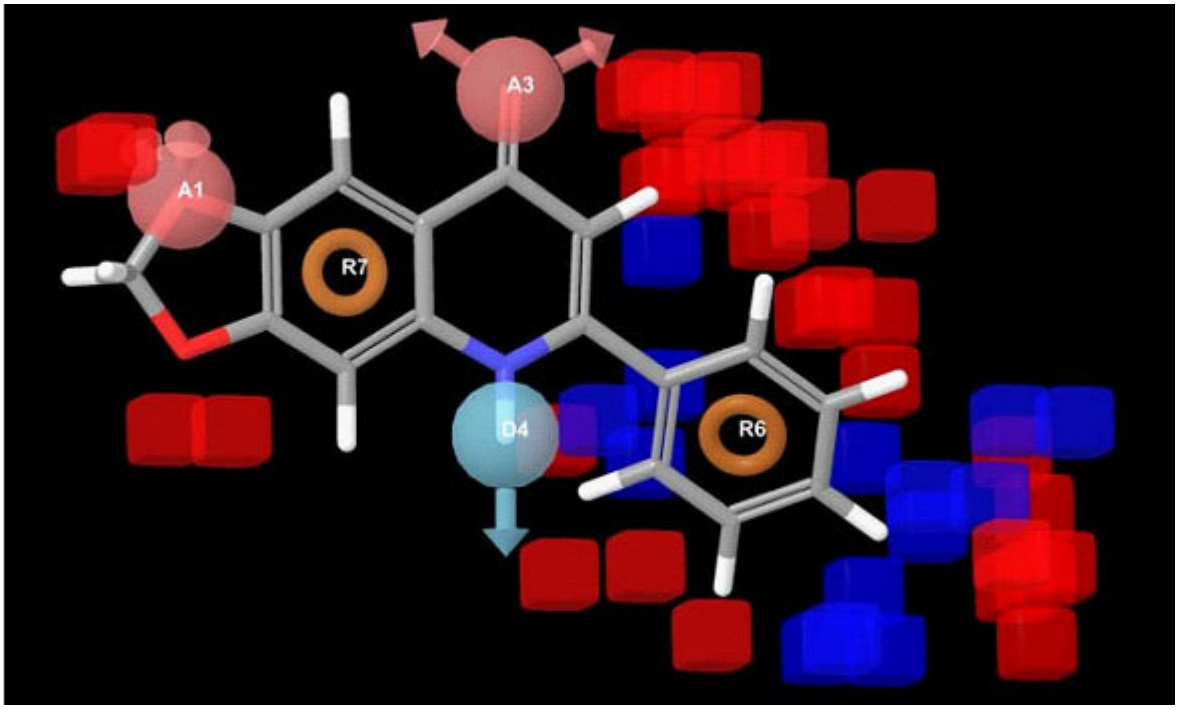

Fig. 4. Pictorial representation of the cubes generated using the 3-D QSAR model based on Comp. no. 1 of training set illustrating hydrophobic feature X CPHs: AADRR.11. Blue cubes indicate favorable regions, while red cubes indicate unfavorable region for the activity

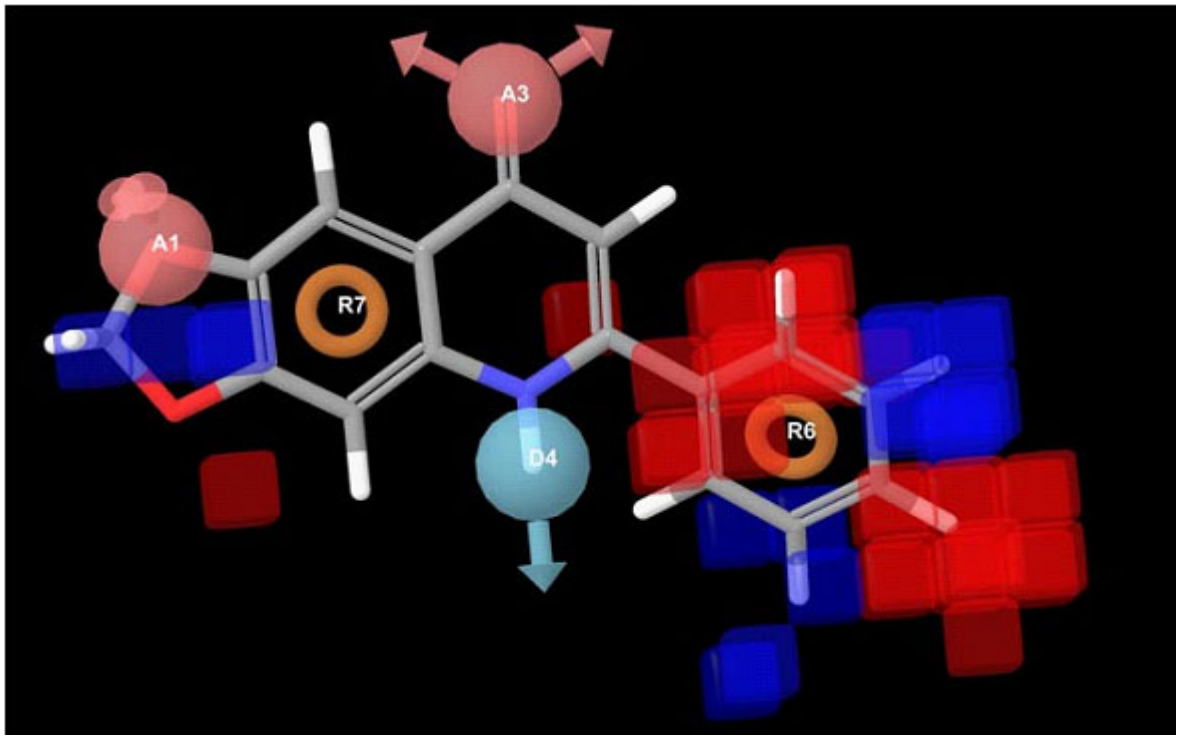

Fig. 5. Pictorial representation of the cubes generated using the 3-D QSAR model based on Comp. no. 1 of training set illustrating hydrogen bond acceptor feature CPHs: AADRR.11. Blue cubes indicate favorable regions, while red cubes indicate unfavorable region for the activity

Hydrogen bond donor field predictions

The 3D-QSAR model based on Comp. no. 1 of the training set using hydrogen bond donor feature is shown in Fig. 3. CPHs AAHRR.11 blue region near the $R_{4¢}$ and D_4 position hydrogen bond donor property favors the antitumor activity so hydrogen donor group at $R_{4¢}$ and D_4 position (NH_2, CH_3) will result in increase in anticancer activity. CPHs red region around the $R_{2¢}$ group and Nitrogen at Quinolones ring hydrogen bond donor property not favors the antitumor activity. So hydrogen donor group (NH_2, CH_3) at $R_{2¢}$ group and Nitrogen at Quinolones ring will result in decline in antitumor activity.

Hydrophobicity field prediction

The 3D-QSAR model based on Comp. no. 1 of the training set using hydrophobicity feature is shown in Fig. 4. CPHs AADRR.11 blue region around $R_{4'}$ and $R_{6'}$ position hydrophobic group favors cell line inhibitory activity and substitutions at these positions by more hydrophobic groups will result in increase in cell line inhibitory activity. Red region around the, $R_{2'}$ $R_{5'}$ and [1,3] dioxolo [4,5g] quinolin 8(5H) one ring at oxygen atom do not favor substitution hydrogen and oxygen with hydrophobic group (CH_3, C_2H_5) with the cell line inhibitory activity.

Hydrogen bond acceptor field prediction

The 3D-QSAR model based on Comp. no. 1 of the training set using hydrogen bond acceptor feature is shown in Fig. 5. CPHs AADRR.11 blue region at $R_{3'}$ $R_{5'}$ and [1,3] dioxolo [4,5g] quinolin 8(5H) one ring at 2 dioxolo (-CH_2-) position, having more hydrogen bond acceptor property favors the antitumor activity. Replace-ment of this group by any electron withdrawing group such as Cl, F, Br, NO_2, OCH_3 etc will result in increase in antitumor activity. Red region around $R_{2'}$ and $R_{4'}$ do not favor the antitumor activity. Replacement of this group by any electron withdrawing group such as Cl, F, Br, NO_2, OCH_3 etc will result in decline in antitumor activity.

Docking studies

Molecular modelling studies were performed to investigate potential interactions for the 4-Quinolones derivatives. The reported X-ray structure of tubulin cocrystallized with a colchicines derivative, N-deacetyl-N-(2 mercaptoacetyl) colchicine (DAMAcolchicine, PDB entry 1SA0) was used for the docking study. Molecular docking studies of parent compound 1 (Figs. 6(a) and 6(b)) predicted similar interactions to those previously reported to be of importance for binding at the colchicine site, including important interactions with Cys241 and Val318. compounds are orientated in a similar manner to DAMA-colchicine, with the 3,4,5-trimethoxyaryl A ring and 4-methoxyaryl B ring occupying the same position in the binding pocket (Fig. 7).

ADME studies

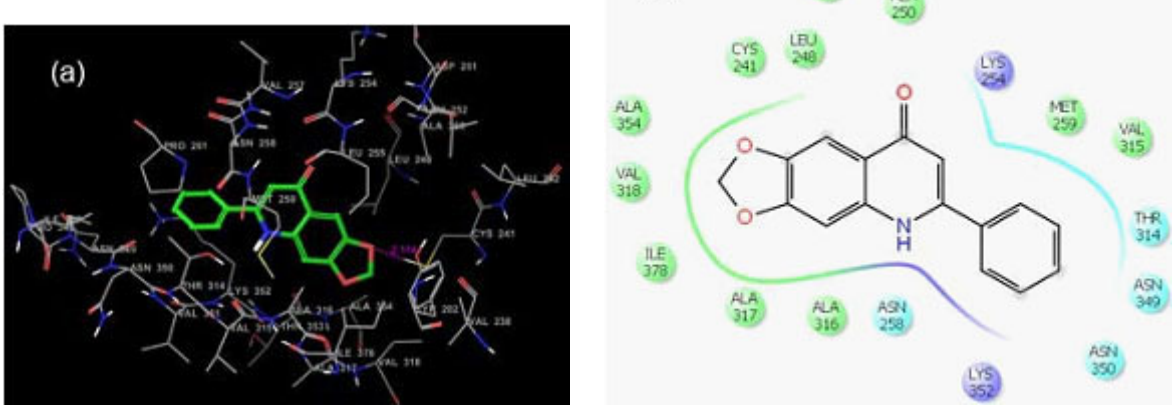

Fig. 6. Docking of compounds on colchicine-binding site of â tubulin Pink dotted lines show hydrogen binding with CYS 241 (a) Docking pose (XP) of Comp. 1 docked (b) 2D representation of the binding interactions of Comp. 1 with the colchicine binding site of tubulin

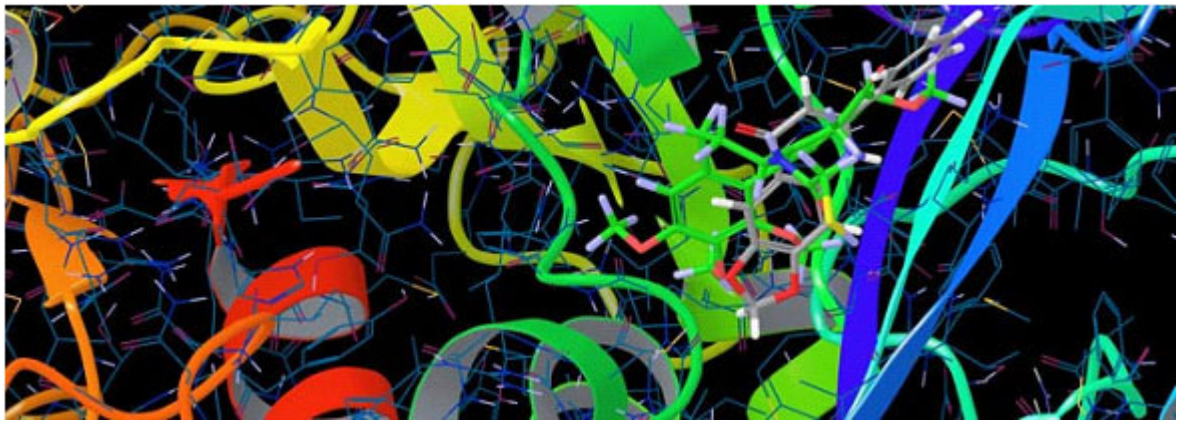

Fig.7. Overlap of colchicines ligand and comp. 1 at binding site. Green color show colchicines ligand and grey color show Comp. 1. The protein structure originated from the X-ray study of its complex with DAMA-colchicine encoded as 1SA0 in PDB) tubulin is shown in a ribbon representation

Prediction of ADME parameters earlier to experimental studies is one of the most imperative features in the drug discovery and development of drug molecules. 43 physical descriptors and pharmaceutically pertinent properties of 4-Quinolone series were analyzed using Qikprop, among which important descriptors are presented in Table 5. These descriptors are necessary for predicting drug-like properties of molecules. These properties were:

1. Molecular weight (mol MW) (180-500)
2. Octanol/water partition coefficient (log P o/w) (-0.4 to +5.4)
3. Aqueous solubility (QPlog S) (-6 to 0.5)
4. Hydrogen bond donors (Not more than 5)
5. Hydrogen bond acceptors (Not more than 10)
6. Apparent MDCK cell permeability (QPPMDCK) (<25 poor)
7. Brain/blood partition coefficient (QPlogBB) (-3.0 to 1.2) Percent human oral absorption (>80 % is high, <25 % are poor)

The first five properties are based on Lipinski rule of five, molecular weight (mol MW) and partition coefficient between octanol, water solubility, Hydrogen bond donor and acceptor. Brain/blood partition coefficient (QlogBB) parameter represents the ability of a drug to pass through blood-brain barrier, whereas QPPMDCK predicted apparent MDCK cell permeability in nm/s. Higher the value of MDCK cell higher the cell permeability.

The physical descriptors and pharmaceutically pertinent properties of 4-Quinolone series were analyzed using Qikprop. The outcomes are as follows: Molecular weight (240 to 357), log P o/w (2.039 to 4.139), QPlog S (-5.028 to -2.795), Hydrogen bond donors (1 to 2), Hydrogen bond acceptors (3.25 to 6.25), QPPMDCK (361.845 to 3237.059), QPlogBB (-0.696 to 0.144) and Percent human oral absorption (92.377 to 100) (Table 5). All the physical descriptors except Apparent MDCK cell permeability (QPPMDCK; it is more than 25 in all the compounds; it should be lesser than 25) represent the promising values for design of 4-quinolones based analogues for potential tubulin polymerization inhibitory activity.

Conclusion

The five feature 3D-QSAR models were developed using variant CPHs which comprises of acceptor, donors, and hydrophobic vector characteristics. The correctness and capability of both 3D-QSAR models were validated internally by applying to test set and externally by predicting the activity of compounds having 4-Quinolones pharmacophore from literature. The one predictive 3D-QSAR models was selected based on statistical results**.** These 3D-QSAR models impart an insight into the structural prerequisite of 4-Quinolones analogs as tubulin inhibitor agents for antitumor activity.

Table 5. Qikprop studies with physical descriptors of 4-Quinolone derivative

Comp.	mol MW Po/w	QPlog	QPlogS	donor HB	accpt HB	QPPMDCK	QPlog BB	Percent Human Oral Absorption
1	265.268	2.589	-3.264	1	4	1317.475	-0.029	100
2	295.294	2.685	-3.497	1	4.75	1317.213	-0.108	100
3	295.294	2.685	-3.482	1	4.75	1316.105	-0.106	100
4	295.294	2.732	-3.589	1	4.75	1286.377	-0.122	100
5	357.365	4.139	-5.028	1	4.5	1317.37	-0.215	100
6	308.336	3.01	-4.109	1	5	1269.354	-0.146	100
7	308.336	3.01	-4.093	1	5	1268.637	-0.145	100
8	279.295	2.89	-3.821	1	4	1317.404	-0.049	100
9	325.32	2.825	-3.792	1	5.5	1315.075	-0.191	100
10	325.32	2.769	-3.717	1	5.5	1316.437	-0.185	100
11	325.32	2.807	-3.777	1	5.5	1286.253	-0.198	100
12	325.32	2.805	-3.788	1	5.5	1286.858	-0.2	100
13	309.278	2.147	-2.866	1	5.5	1318.93	-0.008	100
14	355.346	2.916	-3.854	1	6.25	1315.484	-0.255	100
15	355.346	2.974	-3.759	1	6.25	1454.597	-0.205	100
16	283.258	2.764	-3.528	1	4	1974.243	0.044	100
17	299.713	3.007	-3.843	1	4	2675.813	0.1	100
18	264.326	3.469	-4.531	1	3.5	1263.948	-0.167	100
19	264.326	3.469	-4.548	1	3.5	1264.67	-0.169	100
20	251.284	3.134	-3.9	1	3.25	1311.242	-0.13	100
21	311.337	3.402	-4.379	1	4.75	1310.877	-0.28	100
22	281.31	3.224	-4.164	1	4	1317.393	-0.209	100
23	324.379	3.69	-5	1	5	1268.723	-0.323	100
24	311.337	3.21	-4.32	1	4.75	1316.16	-0.285	100
25	341.363	3.483	-4.726	1	5.5	1315.351	-0.368	100
26	281.31	3.232	-4.148	1	4	1314.823	-0.207	100
27	267.284	2.389	-3.639	2	4	361.845	-0.696	92.377
28	285.729	3.626	-4.651	1	3.25	3237.059	0.03	100
29	269.275	3.369	-4.278	1	3.25	2372.422	-0.022	100
30	296.368	3.452	-4.92	1	4.75	1375.09	-0.147	100
31	283.326	3.202	-4.708	1	4.5	1419.711	-0.131	100
32	254.245	2.097	-3.159	2	4	819.64	-0.121	96.549
33	255.229	2.039	-2.795	1	4.5	1307.408	0.048	100
34	271.29	2.485	-3.481	1	4	2253.017	0.144	100
35	304.304	2.314	-3.599	1	5.5	742.965	-0.188	100
36	240.236	2.686	-3.616	1	3.5	1752.407	-0.057	100
37	240.236	2.664	-3.517	1	3.5	1671.003	-0.046	100
38	252.272	2.55	-3.488	1	4.25	971.336	-0.243	100
39	256.691	2.94	-3.979	1	3.5	2390.265	-0.007	100
40	291.306	3.202	-3.957	1	4	1092.269	-0.262	100
41	291.306	2.956	-3.808	1	4	1696.925	0.121	100
42	321.332	3.052	-4.037	1	4.75	1697.221	0.045	100
43	305.332	3.251	-4.148	1	4	1829.567	0.144	100

Visualization of the 3D-QSAR model gives the details about relationship between structure and the design activity among these molecules and thus provides precise indications about better analogues. Furthermore, the activity-based cubes generated, using 3D-QSAR model along with finally obtained pharmacophoric features, strongly communicates picture of probable active site of the target and can be used as a constructive tool for the rational drug design process. The results of this study are expected to be beneficial for balanced modification of ligands as potential tubulin polymerization inhibitors with good antitumor activity, which can be attained by incorporating predicted structural features to the molecule.

Docking studies were carried out and also correlated with CPHs, which indicated that all compounds bind in similar pose at colchicine binding site of β tubulin. Docking studies provides clear indication about the hydrogen binding of compounds with CYS 241. Subsequent ADME studies disclosed the pharmacokinetic efficiency of these compounds. In conclusion, the overall study provides comprehensive structure and vital binding information of 4-Quinolones derivatives as tubulin binding agents for antitumor activity. Further research studies are under process for complete optimization of various physical descriptors especially Apparent MDCK cell permeability for obtaining 4-quinolones based analogues with promising tubulin polymerization inhibitory activity.

Acknowledgment

We are highly thankful to UGC, New Delhi, India for providing financial assistance in the form of Major Research Project in the area of "combretastatins A-4 analogues as anticancer agents"

Reference

1. **Beckers, T. and Mahboobi, A. (2003).** Natural semi synthetic and synthetic microtubule inhibitors for cancer therapy. Drugs Future. 28: 767-785.
2. **Li, Q. and Sham, H.L. (2002).** Discovery and development of antimitotic agents that inhibit tubulin polymerisation for the treatment of cancer. Expert. Opin. Ther. Pat. 12: 1663-1702.
3. **Prinz, H. (2000).** Recent advances in the field of tubulin polymerization inhibitors. Expert Rev. Anticancer Ther. 2: 695-708.
4. **Checchi, P.M., Netlles, J.H., Zhou, J., Snyder, P., Joshi, H.C. (2003).** Microtubule-interacting drugs for cancer treatment. Trends Pharmacol. Sci. 24: 361-365.
5. **Lin, M.C., Ho, H.H., Pettit, G.R., Hamel, E. (1989).** Antimitotic natural products combretastatin A-4 and combretastatin A-2: studies on the mechanism of their inhibition of the binding of colchicine to tubulin. Biochem. 28: 6984-6991.
6. **Li, L., Wang, H.K., Kuo, S.C., Shung, F.T., Lednicer, I.D., Lin, C.M., Hamel, E., Lee, K.H., (1994).** Antitumor agents. 150. 2',3',4',5',5,6,7-substituted 2-phenyl-4-quinolones and related compounds: their synthesis, cytotoxicity, and inhibition of tubulin polymerization. J. Med. Chem. 37: 1126-1135.
7. **Pettit, G.R., Cragg, G.M., Herald, D.L., Schmidt, J.M., (1982).** Isolation and structure of Combretastatin. Can. J. Chem. 60: 1374-1376.
8. **Pettit, G.R. and Singh, S.B. (1987).** Isolation, structure andsynthesis of combretastatin A-2, A-3, and B-2. Can. J. Chem. 65: 2390-2396.
9. **Pettit, G.R., Singh, S.B., Hamel, E., Lin, C.M., Alberts, D.S. (1989).** Isolation and structure of the strong growth and tubulin inhibitor combretastatin A-4. Experientia. 45: 209-211.
10. **Pettit, G.R., Singh, S.B., Niven, M.L., Hamel, E. (1987).** Isolation, structure and synthesis of combretastatins A-1 and B-1, potent new inhibitors of microtubule assembly derived from Combretum caffrum. J. Nat. Prod. 50: 119-131.
11. **Rajak, H., Dewangan, P.K., Patel, V., Jain, D.K., Singh. A., Veerasamy. R., Sharma. P.C.,**

Dixit, A. (2013). Design of combretastatin A-4 analogs as tubulin targeted vascular disrupting agent with special emphasis on their cis-restricted isomers. Curr. Pharm. Design 19: 1923-1955.

12. **Lin, C.M., Singh. S.B., Chu, P.S., Dempcy, R.O., Schmidt, J.M., Pettit, G.R. (1988).** interactions of tubulin with potent natural and synthetic analogs of the antimitotic agent combretastatin: a structure-activity study. Mol Pharmacol 34: 200-208
13. **El-Zayat, A.A.E., Degen, D., Drabek, S., Clark, G.M., Pettit, G.R., Von Hoff, D.D. (1994).** *In vitro* evaluation of the antineoplastic activity of combretastatin A-4, a natural product from *Combretum caffrum* (arid shrub). Anticancer Drugs. 4: 19-25.
14. **Dixon, S.L., Smondyrev, A.M., Knoll, E.H., Rao, S.N., Shaw, D.E., Friesner, R.A. (2006).** PHASE: a new engine for pharmacophore perception, 3D QSAR model development, and 3D database screening: 1. Methodology and preliminary results. Comp. Aided. Mol. Des. 20: 647-667.
15. **Friesner, R.A., Banks, J.L., Murphy, R.B., Halgren, T.A., Klicic, J.J., Mainz, D.T., Repasky, M.P., Knoll, E.H., (2004).** Glide: a new approach for rapid, accurate docking and scoring. 1. Method and assessment of docking accuracy. J. Med. Chem. 47: 1739-1749.
16. **Watts, K.S., Dalal, P., Murphy, R.B., Sherman, W.R., Friesner, A., Shelley, J.C. (2010).** ConfGen: a conformational search method for efficient generation of bioactive conformers. J. Chem. Inf. Model. 50: 534-546.
17. **Jorgensen, W.L., Maxwell, D.S., Tirado-Rives, J. (1996).** Development and testing of the OPLS all-atom force field on conformational energetics of organic liquids. J. Am. Chem. Soc.118: 11225-11236.
18. **Golbraikh, A. and Tropsha, A. (2002).** Predictive QSAR modeling based on diversity sampling of experimental datasets for the training and test set selection. J. Comp. Aided Mol. Des. 16: 357-369.
19. **Golbraikh, A. and Tropsha, A. (2002).** Beware of q2. J. Mol. Graph. Model. 20: 269-273.
20. **Friesner, R.A., Banks, J.L., Murphy, R.B., Halgren, T.A., Klicic, J.J., Mainz, D.T., Repasky, M.P., Knoll, E.H., (2004).** Glide: a new approach for rapid, accurate docking and scoring. 1. Method and assessment of docking accuracy. J. Med. Chem. 47: 1739-1749.
21. **Friesner R. A., Murphy, R. B., Repasky M.P., Frye, L.L., Greenwood, J.R., Halgren, T.A., Sanschagrin, P.C., Mainz, D.T. (2006).** Extra precision glide: docking and scoring incorporating a model of hydrophobic enclosure for protein-ligand complexes. J. Med. Chem. 49: 6177-6196.
22. **Chen, H.M., Lyne, P.D., Giordanetto, F., Lovell, T., Li, J. (2006).** On evaluating molecular-docking methods for pose prediction and enrichment factors. J. Chem. Inf. Model. 46: 401-415.
23. **Warren, G.L., Andrews, C.W., Capelli, A.M., Clarke, B., LaLonde, J., Lambert, M.H., Lindvall, M., Nevins, N., Semus, S.F., Senger, S., Tedesco, G., Wall, I.D., Woolven, J.M., Peishoff, C.E., Head, M.S. (2006).** A critical assessment of docking programs and scoring functions. J. Med. Chem. 49: 5912-5931
24. **Lipinski, C.A., Lombardo, F., Dominy, B.W., Feeney, P.J. (2001).** Experimental and computational approaches to estimate solubility and permeability in drug discovery and development settings. Adv. Drug Deliv. Rev. 46: 3-26.
25. **Oprea, T.I., Davis, A.M., Teague, S.J., Leeson, P.D. (2001**). Is there a difference between leads and drugs? A historical perspective. J. Chem. Inf. Comp. Sci. 41: 1308-1315.